Dewetting Patterns in a Drying Liquid Film

Leonard W. Schwartz,*,[1] R. Valery Roy,* Richard R. Eley,† and Stanislaw Petrash†

*_Departments of Mechanical Engineering and Mathematical Sciences, The University of Delaware, Newark, Delaware 19716;_
and †ICI Paints Research Center, Strongsville, Ohio 44136

Failure of a liquid coating to remain continuous on a substrate that exhibits a significant equilibrium contact angle is a common occurrence in industrial applications. The term "reticulation" is sometimes used to describe the resulting formation of a pattern of defects. The failure may take the form of coating perforations and dewetting, and it may ultimately lead to a set of isolated drops. We present mathematical and experimental results for reticulation. The theoretical and numerical results use a disjoining–conjoining pressure model to represent the substrate energetics. The theory uses the small-slope or "lubrication" approximation and also includes the effects of evaporation and drying of the coating. The model employs a two-component liquid where the viscosity depends on local values of the nonvolatile mixture fraction. A linear analysis for a slightly perturbed uniform layer predicts a most-unstable wavelength and an associated growth rate. These are in approximate agreement with the modeling results. Computations employing the full nonlinear model show the wide variety of patterns that can arise in the drying liquid. These patterns are both qualitatively and quantitatively similar to actual patterns that we observe experimentally. Small defects that are visible in the experiment are used to initiate reticulation in the numerical simulation.   © 2001 Academic Press

Key Words: liquid film; dewetting; mathematical model; drying; pattern formation; reticulation; numerical simulation; surface tension; disjoining pressure; fluid mechanics.

1. INTRODUCTION

Normally, it is desirable for an applied protective or decorative coating to be of uniform thickness, for both aesthetic and functional reasons. It is sometimes desired, however, to produce an effect in the dry coating layer, such as the hammer tone finish often produced for metallic substrates. These nonuniform, textured finishes generally result from the action of surface tension gradients during the drying process, either produced by an additive or by the natural development of such gradients due to differential evaporation of solvents (1–3). Such effects tend to be maximized for baked finishes but generally do not lead to interruptions of the coating integrity. However, if the substrate is low in wettability or nonuniform in energy, or if the coating itself contains particles of low surface energy, the liquid layer is

subject to rupture or dewetting processes, which are accelerated by higher contact angles of the coating liquid with respect to the substrate or to the nonwetting particle. This process of breakup can proceed to the extent of forming discrete droplets, for example, producing a finish resembling water droplets condensed on a cold surface.

More generally, the breakup of a thin liquid layer on a high-contact-angle surface is a common phenomenon in the natural and industrial worlds. It is observed in agricultural spraying operations, especially on plants with waxy leaves. In both gravure printing and photofinishing applications, the effect is generally undesirable and needs to be mitigated or avoided. It is in these latter applications that the term "reticulation" has come to be used to describe the effect (4).

The goal of the modeling effort presented here is an improved understanding of the complex interaction of several physicochemical processes that influence reticulation. We anticipate that this knowledge base will be useful in product and process design. The goal may either be to control the length scales and textures of patterned coating, when this is desired, or, perhaps more commonly, to avoid these effects by substrate preparation or changes in the rate of drying, for example.

Prior experimental and theoretical work has largely been concerned with dewetting processes for very thin polymeric or aqueous films (5–9). Recently, a preliminary report that combines experimental and theoretical work on a heterogeneous substrate has also appeared (10). In all of these works coating layers are thinner than 100 nm, virtually a factor of a thousand smaller than the protective or decorative coatings considered here. A number of these thin film studies are motivated by applications in microelectronics fabrication.

In the next section we present a theoretical model for the evolution of the droplet-forming pattern while rapid drying is taking place. Numerical solutions obtained using the mathematical model will subsequently be compared with observations made in an experiment of a reticulating coating on a heated plate. Coupled partial differential equations for the shape of the liquid surface $h(x, y, t)$ and the coating-layer-averaged resin fraction $c(x, y, t)$ are formulated. These equations are supplemented with an evaporation or drying law and a law that gives the dependence of viscosity on the local mixture composition. When converted to a computational algorithm, the theoretical

model allows the prediction of the reticulating drop pattern until the coating liquid becomes dry and immobile. The droplet formation process is driven by a significant value of equilibrium contact angle θ_e for the coating liquid on the substrate. Angle θ_e is almost constant on the substrate; small imposed "defects" on the substrate trigger the dewetting instability. The position of the defects is an important determinant of the final pattern. Contact angle information is incorporated in the evolution equation by means of a "disjoining pressure" term of a particular form, as explained below. This modeling represents a new application and an extension of our previous work (3, 11, 12). Certain details of the numerical model, including issues of computational efficiency and robustness, will be discussed in Section 3.

The disjoining pressure model, as used here, is known to incorporate an instability mechanism (13, 14). Thus an exactly uniform initial coating layer, when subjected to disturbances, will become undulatory with an initial length scale that is determined by the coating thickness, the value of the surface tension, and the parameters in the model. In cases considered here this length scale is of the order of 1 mm. As will be shown, the length is only minimally influenced by the effect of gravity. The mathematical model idealizes the defects simply as regions of locally high contact angle on an ideally flat substrate. These defects are, in the experiment, small but visible roughly spherical waxy particles that are fixed on the substrate. Wax particle "footprints" on the substrate are approximately circular and appear to have diameters that range from 50 to about 150 μm. Due to the variable particle size, the wax particles sometimes distort the liquid surface as visible "bumps," while others appear to be fully under the surface, yet dewetting is produced in both cases. As the coating evaporates, the liquid thickness above the particles gets smaller until the coating ultimately dewets at each of these sites. Thus the mathematical model simulates the processes of dewetting, nucleation, and growth of dry patches without actually incorporating complex details of the particle shapes.

Other destabilizing mechanisms due to developed surface tension gradients arising from either thermal gradients during drying or compositional changes, i.e., so-called thermal or solutal Marangoni effects, could also influence the initial instability (15). However, it is remarkable that the experimental patterns are well reproduced using only the observed locations of the small deposited waxy particles. Therefore, we conclude that Marangoni effects are not of significant importance, and they have not been included in the present model.

Section 4 compares predictions of the model with the results of the experiment. In the experiment a liquid coating layer containing the small waxy particles was deposited on an aluminum plate that had been previously coated so as to provide about a 30° contact angle for the liquid. Starting from a continuous layer of liquid, the coating is seen to break up into a pattern of droplets as it dries. The drying is quite fast so as to faithfully reproduce typical industrial conditions that use forced drying to maintain a rapid production rate. Frames taken from a video of the experiment are observed to be strikingly similar to the

simulation results. Exact details of the evolving patterns depend strongly on the initial locations of those waxy particles that serve as nucleation sites. For this reason, differences between the experiment and the simulation generally increase as time proceeds. In both the experiment and the model prediction, drying terminates the motion before a full set of discrete droplets can form. We then alter the drying rate in the simulation so as to give extra time for pattern formation. Two different disjoining-pressure laws are used. For one of these the resulting final pattern for this case does exhibit well-formed final droplets, while, for the other, the liquid solidifies before drop formation is complete. At early times, for the slow-drying case, nucleation and growth of holes in the film can be seen. Similar early-stage hole production has recently been demonstrated numerically in the modeling work of Khanna and Sharma (14).

Concluding remarks and possible extensions of this work are given in Section 5.

2. THE MATHEMATICAL MODEL

Invariably, the thickness of a liquid film or coating is much smaller than characteristic lengths in the filmwise direction. Thus an important simplification is to assume that the coating properties are constant across the thin dimension. This is plausible because the coating layer is very thin and diffusional mixing of the mixture components across this small distance can be expected to happen more rapidly than changes along the film. This "well-mixed" assumption has previously been used in two-dimensional flow models by us and others (2, 16). Not all coating mixtures can be expected to be consistent with this model. Coatings that develop a significant "skin" above a fluid underlayer as they dry would require use of a more complicated model than that presented here.

The thickness profile of the liquid coating layer on a planar substrate is represented by the function $h(x, y, t)$, where x and y are orthogonal coordinates measured along the substrate and t is time. The equation expressing conservation of mass is

$$h_t = -\nabla \cdot \mathbf{Q} - E, \qquad [1]$$

where the rate of evaporation $E(x, y, t)$ has the dimensions of speed. Subscripts signify differentiation. The differential operator ∇ is two-dimensional in the coordinates (x, y). Using the slow-flow and small-slope approximations to the Navier–Stokes equations, i.e., the so-called "lubrication approximation," and assuming an incompressible Newtonian liquid, the flux rate $\mathbf{Q}$ is proportional to the pressure gradient. Applying the no-slip boundary condition on the substrate and assuming zero stress on the liquid–air interface, the resulting expression is

$$\mathbf{Q} = -\frac{h^3}{3\mu}\nabla p, \qquad [2]$$

where $\mu(x, y, t)$ is the viscosity. Both p and μ are assumed to be constant across the thin liquid film. The pressure p includes

capillary and disjoining contributions; i.e.,

$$p = -\sigma \nabla^2 h - \Pi. \qquad [3]$$

The first term on the right of (3) is the capillary pressure where the curvature of the liquid–vapor interface has been simplified using the small-slope approximation. The error in this curvature approximation is proportional to the square of the surface inclination. Here, σ is surface tension and Π is the so-called disjoining pressure as introduced by Frumkin (17) and Deryaguin (18). It is given here by the two-term model

$$\Pi = B\left[\left(\frac{h_*}{h}\right)^n - \left(\frac{h_*}{h}\right)^m\right], \qquad [4]$$

where B and the exponents n and m are positive constants with $n > m > 1$. The local disjoining energy density

$$e^{(d)}(h) = -\int_{h_*}^{h} \Pi(h') \, dh' \qquad [5]$$

has a single stable energy minimum at the thin precursor-layer thickness $h = h_*$. In general, h_* is small compared to the average or initial coating thickness h_0. In the dynamic simulations presented here, h_* plays the role of a "slip coefficient" allowing motion of the apparent contact lines where a thick coating layer meets a dry portion of the substrate. Because the disjoining pressure is assumed to depend only on the local interfacial separation h, the validity of expressions such as [4] and [5] also requires the small-slope approximation.

For a drop at static equilibrium whose surface meets the substrate at an apparent equilibrium contact angle θ_e, it is possible to relate θ_e to the constants in expression [4]. By performing a force balance in the neighborhood of the apparent contact line, and assuming that h_* is very small, it may be shown that

$$B = \frac{(n-1)(m-1)}{h_*(n-m)} \sigma(1 - \cos\theta_e)$$
$$\approx \frac{(n-1)(m-1)}{2h^*(n-m)} \sigma\theta_e^2, \qquad [6]$$

where the approximate equality assumes that the contact angle is small. It is also possible to show that

$$e^{(d)}(\infty) = \gamma_{LV} + \gamma_{SL} - \gamma_{SV}, \qquad [7]$$

where $e^{(d)}(\infty)$ is calculated from (4) and γ_{SL}, γ_{SV} and $\gamma_{LV} = \sigma$ are the interfacial tensions, or interfacial energy densities, where the solid (S), liquid (L), and vapor (V) meet at the apparent contact line. The detailed derivation leading to [6] and [7] may be found elsewhere (12).

The final form of the evolution equation for the coating thickness, including capillarity, substrate energetics, and evaporation,

is found by combining [1] to [4] and [6] to yield

$$h_t = -\frac{\sigma}{3\mu} \nabla \cdot \left[h^3\left(\nabla\nabla^2 h + \frac{(n-1)(m-1)\theta_e^2}{2h_*(n-m)}\right.\right.$$
$$\left.\left. \times \nabla\left[C(x,y)\left(\frac{h_*^n}{h^n} - \frac{h_*^m}{h^m}\right)\right]\right)\right] - E. \qquad [8]$$

The function $C(x, y)$ allows for the possibility that the contact angle may vary on the substrate. For a uniform substrate $C = 1$.

We use a relatively simple drying model but require that it incorporate the following basic properties:

(i) As the coating dries, material is lost.
(ii) The viscosity of the coating increases as it dries.
(iii) The coating dries more quickly in thin regions.
(iv) The reticulation process is a competition between the interfacial energetics that drive reticulation and drying which slows and ultimately stops the motion.

We consider the coating to be a mixture of two components, a volatile solvent and a nonevaporating resin. The viscosity is a function of the local concentration or resin fraction $c(x, y, t)$ that increases as the coating dries. Initially, before any evaporation has taken place, the liquid is assumed to have uniform composition. Thus the initial condition for the resin fraction is $c(x, y, 0) = c_0$, where $c_0 < 1$, the initial resin fraction, is a prescribed constant. The function $\mu(c)$ is taken to be of the form

$$\mu = \mu_0 \exp[a(c - c_0)], \qquad [9]$$

where the constant a is sufficiently large so that the viscosity of a dry coating ($c = 1$) is effectively infinite; then the dried coating will be immobile.

As the coating dries the rate of evaporation can be expected to decrease. The postulated drying law is

$$E = E_0(1 - c)^\nu, \qquad [10]$$

where E_0 is the drying rate for pure solvent, which may be expected to be virtually constant in a well-ventilated environment. The exponent ν is in the range

$$0 \le \nu < 1.$$

This restriction on the drying law exponent is made clear by considering drying of a uniform layer, initially at thickness h_0. The evolution equation is then simply

$$\frac{dh}{dt} = -E = -E_0(1 - c)^\nu \qquad [11]$$

Since the resin is nonvolatile, we must have $ch = c_0 h_0$; thus [11] becomes

$$\frac{c_0 h_0}{E_0} \frac{dc}{dt} = c^2(1 - c)^\nu,$$

which may immediately be integrated to find the drying time,

$$\frac{E_0}{c_0 h_0} t_{\text{dry}} = \int_{c_0}^{1} \frac{dc}{c^2(1-c)^{\nu}}.$$ [12]

In order for t_{dry} to be finite, the integral must be convergent, which requires that ν be strictly less than one. The evaporation model given above is highly simplified; other factors that may influence evaporation are discussed by Sharma and colleagues (19, 20).

The concentration is a second unknown function of space and time; thus a second evolution equation must be solved simultaneously with [1]. This is done most easily by defining a "resin height" as

$$h_{\text{R}} \equiv ch.$$ [13]

Because the coating is assumed to be well mixed across the thin film, the resin flux is given by

$$\mathbf{Q}_{\text{R}} = c\mathbf{Q}.$$ [14]

Since the resin is nonvolatile, the resin evolution equation is simply

$$h_{\text{R}t} = -\nabla \cdot \mathbf{Q}_{\text{R}} = -\nabla \cdot (c\mathbf{Q}).$$ [15]

Using Eqs. [2], [3], and [13], this may be rewritten as

$$h_{\text{R}t} = -\nabla \cdot \left[\frac{ch^3}{3\mu} \left(\sigma \nabla \nabla^2 \frac{h_{\text{R}}}{c} + \nabla \Pi \right) \right].$$ [16]

As an alternative to Eq. [16], Eqs. [1] and [13] through [15] can be combined to form the concentration equation

$$\frac{\partial c}{\partial t} + \frac{\mathbf{Q}}{h} \cdot \nabla c \equiv \frac{\partial c}{\partial t} + \mathbf{u} \cdot \nabla c \equiv \frac{Dc}{Dt} = \frac{cE}{h},$$ [17]

where $\mathbf{u}$ is the layer-average velocity and D/Dt is the convective derivative, i.e., the time derivative following the motion of a fluid element. While formally equivalent to [16], Eq. [17] is not in divergence or "conservation form." Thus the finite-difference form of [17] will not exactly conserve the total amount of resin in a time-marching numerical algorithm. In order to maintain this important property, Eq. [16] will be used instead of [17].

Because the coating dries more quickly in relatively thin regions, the two-component liquid will develop concentration gradients as it dries. These gradients are partially mitigated by diffusive mixing. Assuming Fickian diffusion, the diffusional flux of resin is

$$\mathbf{Q}_{\text{R}}^{(\text{D})} = -Dh_{\text{R}} \nabla c$$ [18]

where the diffusion constant D may be a function of the concentration c. The divergence of the diffusional flux is appended to the resin evolution equation [16].

The equations are solved in dimensionless variables using the initial wet-film thickness h_0 and the initial viscosity μ_0 as reference quantities. The transformation to dimensionless. i.e., tilded, variables is

$$h = h_0 \tilde{h}, \quad (x, y) = L(\tilde{x}, \tilde{y}), \quad t = T^* \tilde{t}.$$ [19]

The characteristic time is

$$T^* = \frac{3\mu_0 L^4}{\sigma h_0^3},$$

while L is chosen to be a characteristic length for pattern formation, as discussed below. The h-evolution equation, using these dimensionless variables, is

$$\tilde{h}_{\tilde{t}} = -\tilde{\nabla} \cdot \left[\frac{\tilde{h}^3}{e^{a(c-c_0)}} (\tilde{\nabla}\tilde{\nabla}^2 \tilde{h} + \tilde{\nabla}(\tilde{C}\tilde{\Pi})) \right] - \tilde{E}_0(1-c)^{\nu},$$ [20]

where

$$\tilde{\Pi} \equiv \left(\frac{h_*}{h} \right)^n - \left(\frac{h_*}{h} \right)^m.$$

The dimensionless resin evolution equation becomes

$$\tilde{h}_{\text{R}\tilde{t}} = -\tilde{\nabla} \cdot \left[\frac{c\tilde{h}^3}{e^{a(c-c_0)}} \left(\tilde{\nabla}\tilde{\nabla}^2 \frac{\tilde{h}_{\text{R}}}{c} + \tilde{\nabla}(\tilde{C}\tilde{\Pi}) \right) \right]$$
$$+ \tilde{\nabla} \cdot \left(\tilde{D}\tilde{h}_{\text{R}} \tilde{\nabla} \frac{\tilde{h}_{\text{R}}}{\tilde{h}} \right).$$ [21]

Equations [20] and [21] along with the definition $h_{\text{R}} = ch$ constitute the basic model.

The independent parameters that appear in the model are

$$n, m, \tilde{C} = \frac{f_{nm}\theta_{\text{e}}^2 L^2}{h_0 h_*}, \quad \tilde{E}_0 = \frac{T^* E_0}{h_0}$$ [22a]

and

$$a, c_0, \nu, \frac{h_*}{h_0}, \tilde{D} = \frac{D}{L^2/T^*}.$$ [22b]

The factor that appears in the definition of $\tilde{C}$ is

$$f_{nm} = \frac{(n-1)(m-1)}{2(n-m)}.$$

Various extensions to the basic model are possible and have been implemented in related work. Rather than use a constant resin diffusivity, it is possible to make the diffusion constant $\tilde{D}$ an inverse function of the local viscosity which depends, in turn,

on the concentration c. To the extent that resin diffusion is due to Brownian motion, $\tilde{D}$ would be inversely proportional to μ as in the Einstein model of Brownian motion. This is discussed, for example, by Landau and Lifshitz (21). We have made this simple modification in earlier work involving a two-component liquid mixture. Similarly the surface tension need not be constant but could be a function of the resin fraction. This is known to be the case for certain coatings such as alkyd paints (1). Because a nonuniform liquid layer dries unevenly, gradients of surface tension will arise during drying for these coatings. A simple force balance on the liquid surface shows that the surface tension gradient is equivalent to an applied shear stress that will drive liquid motion. This is the so-called *solutal Marangoni effect*. Both effects have been included in Eres *et al.* (3) in their model for the shape evolution of a drying paint layer. In the simulation of the experiment considered here, liquid motion is ultimately controlled by rapid drying. Thus species diffusion has only a minor effect, and Marangoni effects, if present at all, will be minimal. Consequently, use of the more sophisticated model is not warranted.

In the dimensionless model, the spatial length scale L is chosen to be the wavelength of maximum growth of a small-amplitude sinusoidal disturbance that is imposed on an otherwise uniform layer. This length should then be representative of the most likely initial spacing between mounds or ridges in the developing surface pattern. A simple stability analysis can be employed to determine L. Equation [8] can be considerably simplified if we only consider the stability of a uniform layer of liquid of thickness h_0 to a spatially one-dimensional perturbation; thus the two-dimensional operator ∇ is replaced by $\partial/\partial x$. Evaporation may also be neglected and we consider the substrate to be uniform; thus $C = 1$. For $h_* \ll h_0$, we have

$$C\left(\frac{h_*^n}{h^n} - \frac{h_*^m}{h^m}\right) \approx -\frac{h_*^m}{h^m} \quad [23]$$

because $n > m$. Let

$$h = h_0 + h_1 \quad [24]$$

and assume that

$$|h_1| \ll h_0.$$

Defining

$$A = \frac{(n-1)(m-1)\theta_e^2}{2h_*(n-m)},$$

the equation governing the perturbed height h_1, i.e., the linearized form of [8], becomes

$$h_{1t} = -\frac{\sigma h_0^3}{3\mu_0}\left[h_{1xxxx} + \frac{mAh_*^m}{h_0^{m+1}}h_{1xx}\right]. \quad [25]$$

This equation is satisfied by solutions of the form

$$h_1 = \text{const} \cdot e^{\omega t}\cos kx, \quad [26]$$

where k is a wavenumber and ω is a disturbance growth rate. Substituting in [25], the growth rate depends on wavenumber according to

$$\omega = -\frac{\sigma h_0^3}{3\mu}\left[k^4 - \frac{mAh_*^m}{h_0^{m+1}}k^2\right]. \quad [27]$$

The wavenumber of maximum growth k_{max} satisfies

$$\frac{\partial\omega}{\partial k} = 0,$$

yielding

$$k_{max}^2 = \frac{mAh_*^m}{2h_0^{m+1}}. \quad [28]$$

Finally, the predicted wavelength that grows most rapidly, corresponding to the most likely initial spacing between mounds or ridges, is

$$L \equiv \frac{2\pi}{k_{max}} = \frac{4\pi h_0}{\theta_e}\sqrt{\frac{n-m}{(n-1)(m-1)m}\left(\frac{h_0}{h_*}\right)^{m-1}}, \quad [29]$$

where the previously defined intermediate quantity A has been restored. The growth rate of disturbances with wavelength L is then

$$\omega_{max} = \frac{\sigma\theta_e^4}{48\mu_0 h_0}\left[\frac{(n-1)(m-1)m}{n-m}\right]^2\left(\frac{h_*}{h_0}\right)^{2m-2}. \quad [30]$$

The analysis leading to Eqs. (29) and (30) can also be extended to consider the effect of gravity when the coating is applied on top of a horizontal substrate. For simplicity, the result is only given for the special choice of disjoining exponents $(n, m) = (3, 2)$. With gravity included, the growth rate relation, replacing [27], is

$$\omega = -\frac{\sigma h_0^3}{3\mu}\left[k^4 - \left(2\theta_e^2\frac{h_*}{h_0^3} - \frac{1}{L_c^2}\right)k^2\right]. \quad [31]$$

Here, $L_c = \sqrt{\sigma/(\rho g)}$ is usually called the capillary length. As before, the wavelength of most rapid growth and the corresponding rate can be calculated easily using [31]. Additional destabilizing effects in thin liquid films that are associated with evaporation are discussed by Oron *et al.* (22).

A number of parameters that appear in [29] and [30] can be considered known. These are the initial viscosity μ_0, the surface tension σ, the equilibrium contact angle θ_e, and the wet coating thickness h_0. Equation [29] predicts that the dimensions of

features in the final pattern can be expected to be proportional to the coating thickness and to vary inversely with the contact angle. Similarly [30] predicts that characteristic growth rates for pattern formation will increase strongly with substrate contact angle and will be reduced by large viscosity and large coating thicknesses. The two exponents (n, m) and the "disjoining" equilibrium thickness ratio h_*/h_0 are less clear, however. Relatively large values of of n and m can be seen to act similarly to small values of h_*. We will choose, for most of the present simulations, the values $(n, m) = (3, 2)$ and $h_*/h_0 = 0.10$. This choice will be shown to produce very credible behavior when compared with the experiment. With gravity included, the fastest growing wavelength and the corresponding rate are changed by less than 1% and less than 3%, respectively. Consequently, gravitational effects can safely be ignored for the present purpose.

3. COMPUTATIONAL ISSUES

Equations [20] and [21] are solved using time-marching finite-difference methods. Straightforward explicit time-marching schemes for diffusive equations of this type require that time steps be very small in order to maintain numerical stability. As in the model equation

$$h_t = -h_{xxxx},$$

a requirement is that Δt be less than a small constant multiple of $(\Delta x)^4$, where Δx is the space step or mesh size. Thus the computational requirement quickly becomes more severe as the mesh size becomes small for an explicit method. We have found that the order of magnitude of Δx must be that of the disjoining-layer thickness h_* or smaller, in dimensionless units. In order to overcome this time step size limitation, the three-dimensional solutions given here use an alternating-direction-implicit (ADI) technique (23–25). ADI uses alternating sweeps in each direction, and a banded system of equations is solved to update the discrete set of $h_{i,j}$ or $h_{Ri,j}$ values in a "row" or "column" of the computational domain. Maximum permissible time steps are much larger than the characteristic maximum step for stability for an explicit method. Apparent "contact lines," where the thick liquid layer meets the disjoining layer, are captured by the method, and their motion appears as part of the evolving solution. Nonlinear prefactors in the equations are evaluated at the previous time level.

It has been found that an adaptive time-stepping procedure, where the time step is adjusted dynamically based on a preset maximum permissible change in any h value, greatly increases computational efficiency. Motions with strong capillary effect often exhibit alternating slow and rapid events as the liquid pattern evolves. Thus a time integration scheme that is able to adapt to these changes is particularly appropriate. Temporal convergence is verified by reducing the allowed maximum change in h. Further details of the basic numerical methods employed here may be found elsewhere (3, 26, 27).

We also require that the algorithm satisfy what may be called a "mixing property," i.e., that mixing caused by flow alone can never produce new extrema of the resin concentration $c(x, y, t)$. More simply, the mixing property states that, locally, the concentration at a point at the updated or "new" time cannot be less than (greater than) the minimum (maximum) concentration at its neighboring points at the previous or "old" time. This follows from the fact that the new concentration, after a time step has elapsed, is a weighted average of the old concentrations. Writing the concentration equation [17] in discrete form, ignoring both evaporation and diffusion, and considering motion in only one space dimension, it can be shown that maintenance of the mixing property requires that

$$u \frac{\Delta t}{\Delta x} < 1. \qquad [32]$$

Here u is the layer-average liquid speed which can become relatively large near the edges of drops or holes. Equation [32] is the so-called Courant condition that often arises in finite-difference calculations when convective changes are important.

The computation is performed on a rectangular domain in the (x, y) plane. This domain represents only a portion of the physical substrate used in the experiment. Boundary conditions are required for both the surface profile h and the concentration distribution c. Two choices have been used for these boundary conditions. Periodic boundary conditions assume, for a domain of size L_x by L_y, that

$$h(x + L_x, y, t) = h(x, y + L_y, t) = h(x, y, t),$$
$$c(x + L_x, y, t) = c(x, y + L_y, t) = c(x, y, t). \qquad [33]$$

Thus the entire plane is covered by periodic images of the computational domain. Alternatively, reflection symmetry conditions may be used instead. These are

$$h_n = h_{nnn} = c_n = 0, \qquad [34]$$

where the n subscripts indicate differentiation in the normal direction at each boundary. For the present experimental comparison, we have found the periodic boundary conditions produce fewer features that caused solely by the presence of the computational boundary. The simulation results given below use periodic boundary conditions. When the reflection conditions [34] are used instead, there is a pronounced tendency for non-circular surface features to align their long axes parallel to computation boundaries.

Calculations given here use a uniform rectangular mesh with 90 by 120 mesh intervals. Thus there are about 2.2×10^4 unknowns in the vectors h and h_R. A full calculation, starting from a uniform coating layer and continuing until the coating is dry, takes less than 1 h on a desk-top computer with a Pentium-class processor. The numerical algorithm is programmed in Fortran. The operating system is Linux, a public-domain version of the

Unix operating system. By comparing results using somewhat finer and somewhat coarser meshes, it was verified that the influence of grid size on the computed results shown here is minimal.

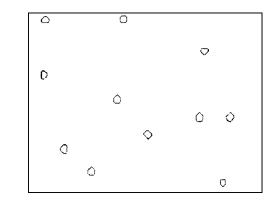## 4. COMPARISON OF MODEL RESULTS WITH EXPERIMENT

Aluminum sheets having dimensions 2 cm by 10 cm and thickness 0.3 mm were used as substrates. The substrates were first coated with blue or white pigmented water-based ink using a second aluminum plate as a spreader. The ink-coated substrate was then baked on a hotplate at 400°F for approximately 30 s. After allowing the substrate to cool, the clear topcoat was then uniformly spread onto the ink-coated surface of the substrate using a glass microscope slide. The liquid coating was comprised of an aqueous thermosetting polymer emulsion system containing waxy particle additives. The thickness of the coating was controlled by the amount of pressure applied to the glass slide. The aluminum plate with ink and wet topcoat was then placed on the surface of the hotplate maintained at a temperature of 400°F. At the same time, video recording was activated to capture the reticulation process. The video camera was mounted on a vertical axis perpendicular to the surface of the substrate. The image was recorded using an S-VHS VCR and was converted to digital format using a video capture card. It required about 10 s total time for reticulation to cease, with solidification of the coating. The topcoat was initially continuous and uniform but rapidly dewetted from the included low-wetting particles to form liquid beads or droplets.

The simulation used the dimensional and nondimensional parameter values given in Table 1. The equilibrium contact angle, the initial viscosity, the surface tension, the initial resin fraction, and the initial coating thickness are experimental values that can each be considered accurate with an error of no more than 10%. The solvent evaporation rate E_0 is estimated using the observed time for immobility of about 10 s. Using the disjoining exponent pair $(n, m) = (3, 2)$, the disjoining thickness h_* was selected so that the instability wavelength L was equal to 2.0 mm. Thus, as observed in the experiment, the initial number of "features" on the 8 mm by 6 mm window shown was about 4 across by 3 wide.

TABLE 1
Parameter Values Used in the Simulation

Physical quantity	Symbol	Value and units
Contact angle	θ_e	0.5 rad or 28.7°
Initial viscosity	μ_0	0.25 p = 0.25 g/(cm s)
Surface tension	σ	35 dyn/cm
Initial coating thickness	h_0	50 μm
Disjoining thickness	h_*	5 μm
Solvent evaporation rate	E_0	2 μm/s
Diffusion constant	$\tilde{D}$	0.1 (dimensionless)
Initial resin fraction	c_0	0.3 (dimensionless)
Viscosity exponent	a	70 (dimensionless)
Evaporation exponent	ν	0.5 (dimensionless)

FIG. 1. The defect pattern used to start the computational model. The location of each defect was taken from observations of wax particles in the experimental video. The contact angle is about 15% larger on the defects.

The dimensionless resin diffusion coefficient given in the table corresponds to the physical value $D \approx 1.4(10^{-5})$ cm^2/s. This is a reasonable estimate for mixing of low-viscosity liquids. Since the experiment happened rapidly, resin diffusion is actually quite unimportant, a fact that was confirmed by simulation runs using very different values of D. The viscosity exponent a from Eq. [9] is essentially determined by the above value of E_0 and the very large value of viscosity that is required for immobility. Finally the evaporation law exponent ν given in the table, and appearing in Eq. [10], is a plausible intermediate value.
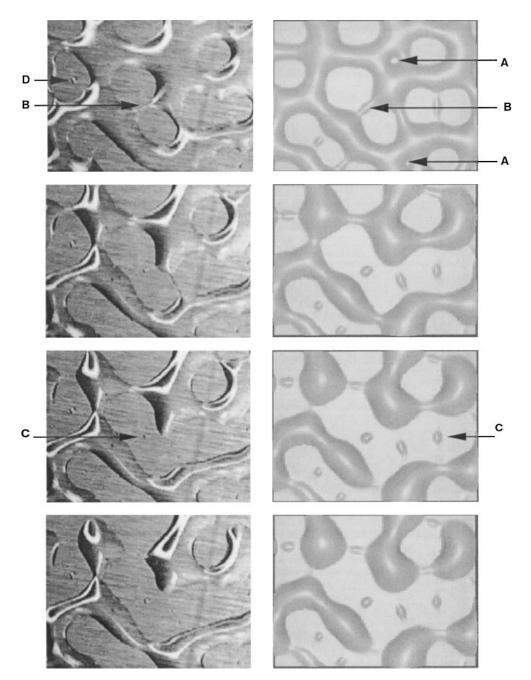
In the video of the experiment, a set of less-wettable waxy particles can be seen at an early stage of the experiment, before the liquid–air interface has deformed appreciably. The observed particle locations were used as disturbance sites for the simulation. Eleven disturbance sites were used in the simulation, each having a diameter of about 0.25 mm. On the disturbance sites the equilibrium contact angle was taken to be about 15% larger than on the surrounding field. This defect pattern is shown in Fig. 1. The initial condition was taken to be a perfectly uniform coating surface and uniform resin concentration. In the simulation, the rate of initiation depends on the intensity of the defects, a quantity that is assigned arbitrarily. Had the intensity been taken to be much smaller, it would have taken longer for the disturbances to grow to recognizable amplitude.

Four frames from the experimental video and the corresponding simulation results are shown in Fig. 2. The three-dimensional simulation images were produced using a public-domain graphics program called Geomview. The sequence of events, which is largely modeled successfully, may be described as follows:

(i) Rippling of the surface, followed by perforation in the vicinity of the imposed defects.

(ii) Expansion of each defect as a circular hole until the holes approach one another. The liquid removed from the holes piles up on the expanding rims.

(iii) The coating between the approaching holes becomes a bridging filament or "dike." Each dike thins as the contained liquid is pumped to the bordering mounds. This local flow is driven
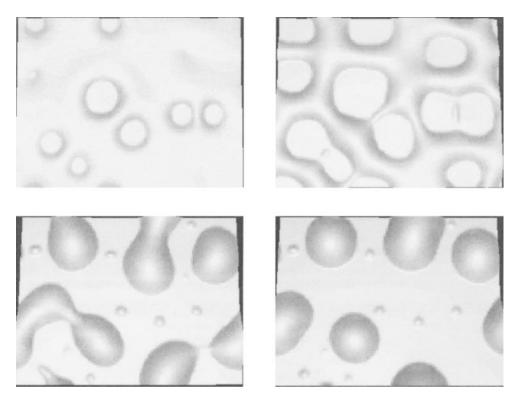
FIG. 2. Comparison of experiment (left) and model simulation (right). The time difference between frames is about 1 s both for the experiment and the simulation. The coating is sensibly immobile at the last times shown for both. The "window" size is 8 mm by 6 mm. See text for values of the physical parameters and feature definitions.

by the higher capillary pressure within the dike. The capillary pressure increases as the radius of curvature decreases.

(iv) The filaments break and typically leave behind isolated small droplets because the filaments break up with a characteristic instability wavelength which is, in general, incommensurate with the length of the filament. Production of these small droplets is a capillary-driven phenomenon; a similar effect leads to the secondary or "satellite" droplets that often form when a thin liquid stream breaks up, as in ink-jet printing, for example. The

location of these small droplets in a final dry coating pattern, therefore, gives information about the previous history of the motion. It is interesting to note that many of the features observed here for thick coating films are similar to corresponding events that are seen in the breakup of very thin polymeric films (7, 6).

The time difference between the pictures in Fig. 2, for both the experiment and the simulation, is 1 s. Particular phenomena are identified by arrows and letters in the figures. The letter "A"

FIG. 3. Simulation results for slower drying. All parameter values are the same as those in the experimental simulation except that the drying rate has been halved. Evolving patterns are shown at $t = 1.0$, 1.3, and 1.9 s. The final pattern for $t > 8$ s is at the lower right. The pattern at 1.3 s is quite similar to the first simulation picture in Fig. 2. The difference is that the secondary indentations, indicated by "A" in Fig. 2, do not form.

shows secondary perforations of the liquid film in the simulation. These minor perforations are transient and do not correspond to initial seed locations. As can be seen, they are soon filled in by the expansion of the larger holes. In both the experiment and the simulation, "B" identifies a liquid filament between expanding holes. When each filament ultimately breaks, a satellite droplet is left behind, indicated by "C." These satellites are somewhat larger in the model, compared to the experiment. Careful inspection of the experimental pictures shows several wax particles, which act as "seeds" or nucleation sites for pattern forming. One of these is indicated by the letter "D."
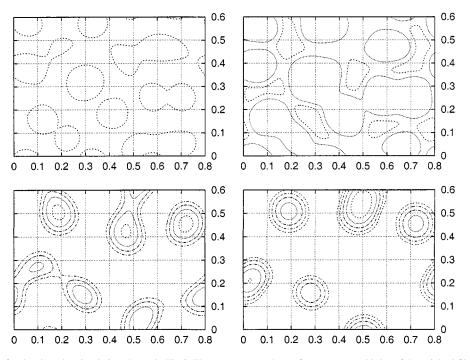
Figure 3 shows evolving patterns for a coating that dries more slowly than that of the experiment. All parameter inputs are the same as those for Fig. 2 except that the initial solvent evaporation rate is $E_0 = 1$ μm/s, one-half the previous value. Because the viscosity remains low for a longer time period, patterns evolve more quickly. The four pictures span a longer pattern-forming interval than those shown in Fig. 2. The first frame, at time $t = 1.0$ s, shows hole initiation and growth with expanding ridges around each hole. The hole locations correlate closely with the seed locations in Fig. 1. The second frame, at $t = 1.3$ s, is quite similar to the first picture in Fig. 2, while the third picture ($t = 1.9$ s) is about the same as the final dry pattern for the more rapidly drying experimental case. The last picture shows the final pattern for this slow-dry case that is realized after 8 s. It shows a number of well-formed isolated drops. If the goal of an

industrial process is to achieve such a pattern, this simulation result has identified an appropriate drying rate.

While the rendered pictures shown in Figs. 2 and 3 give a clear indication of the nature of the patterns, they do not display a high degree of quantitative information about actual film thicknesses. Such information is given by plots of coating thickness contours. Figure 4 shows contour plots of the film thickness for the same times that are shown in Fig. 3. Contours are shown for thicknesses in intervals of 50 μm.
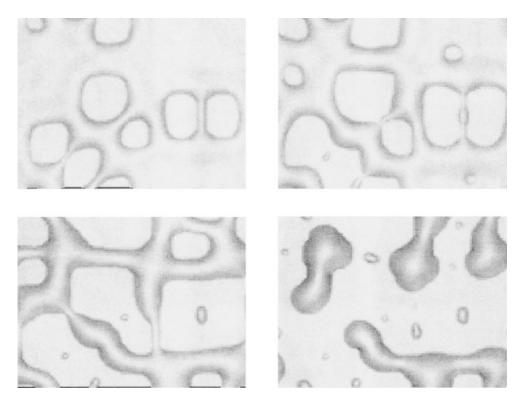
Finally we consider the effect of changing the disjoining exponents on the simulation results. Changing the exponent pair in the disjoining expression [4] will affect the subsequent motion in at least two ways. The "steepness of the energy well" at the equilibrium slip layer thickness $h = h^*$ is given by the second derivative

$$\left[\frac{d^2 e^{(d)}}{dh^2}\right]_{h=h^*} = -\left[\frac{d\Pi}{dh}\right]_{h=h^*} = \frac{\sigma \theta_e^2}{2h^{*2}}(n-1)(m-1) \quad [35]$$

using equations [4], [5], and [6]. Changing the exponent pair from (3, 2) to (4, 3), for example, increases this steepness or curvature by a factor of three. The resulting behavior of apparent moving contact lines will also be changed. Apparent dynamic contact angles will differ less from the static angle during motion; in effect the "stiffness" of the dynamical system will be

FIG. 4. Contour plots for the slow-dry simulation shown in Fig 3. The contours are shown for constant multiples of the original film thickness $h_0 = 50 \ \mu$m. Distances along the substrate are measured in centimeters. Thus, the thickest formed drop in the last figure has a height of about 250 μm and a diameter of about 2 mm.

FIG. 5. Simulation results using the disjoining-model exponent pair $(n, m) = (4, 3)$ rather than $(3, 2)$. All other input parameters are the same as those used for Figs. 3 and 4 except for the defect strength, which has been increased by a factor of five, as explained in the text. The times are the same as in Fig. 3, namely, $t = 1.0, 1.3,$ and 1.9 s; as in Fig 3, the final dry pattern is shown at the lower right.

increased. Further discussion of the dynamical effect of the disjoining exponent choice is given in Ref. (11).

A more immediate effect of the exponent choice concerns the initial rate of growth of unstable disturbances on a uniform coating layer. The stability analysis leading to Eq. [30] indicates that, for the system parameter values given in Table 1, changing the exponent pair from (3, 2) to (4, 3) will reduce this growth rate by about a factor of five. In our simulation, it is the larger value of equilibrium contact angle on the spots shown in Fig. 1 that drives the dewetting pattern formation. In order to preserve the time scale for initial perforation of the coating film, for example, with the reduced growth rate, it is necessary to increase still further the contact angle on the spots. Using Eq. [8], we find that an approximate criterion is that the product of the initial growth rate and the quantity

$$\frac{\theta_{\text{spot}}^2}{\theta_{\text{field}}^2} - 1$$

should be held constant in order to maintain the time scale. For the (4, 3) exponent pair, therefore, the spot contact angle is taken to be 58% larger than the field contact angle. This compares with the previously used 15% value for the (3, 2) case.

Simulation results using the (4, 3) exponent pair are shown in Fig. 5. These four pictures may be compared with the corresponding pictures in Fig. 3. The film perforation patterns are seen to be quite similar at the two earliest times $t = 1.0$ and 1.3 s. Significant differences can be seen at later times, and the final dry configuration for the (4, 3) case shows less complete droplet formation when compared with the (3, 2) case. Ridges separating dry spots appear to be of more-uniform width than for the (3, 2) exponent choice. We believe this effect is associated with the increased "stiffness" of the model as mentioned above. The four stages of pattern formation, as identified in the experiment and the simulation using the (3, 2) pair, can also be seen clearly in the sequence of pictures in Fig. 5.

As stated above, several of the parameter values used in the simulations have been chosen to provide good agreement with the experiment. These are the spot contact angles, the drying rate, and the slip-layer thickness h^*. Minor adjustments in these values would have allowed the simulation using the (4, 3) exponent pair to provide much closer agreement with the experiment. We feel that it is more instructive to show, as we have done, the effect of a change in the exponent pair with all other parameters held constant. The similarities between the simulation frames suggest that the choice of disjoining exponents affects quantitative rather than qualitative features, and is a less important determinant of dewetting patterns than many of the other input quantities.

5. CONCLUDING REMARKS

A mathematical and numerical model has been developed for the evolution of a thin liquid coating layer on a low-energy sub- strate. The coating forms particular patterns of holes, ridges, filaments, and, ultimately, droplets as it dries. Most of the features exhibited by the model are also seen in videos taken from an experiment. While the agreement between the model and experimental results is generally quite good, there are some differences which can be attributed to the various simplifications employed in developing the model. The experimental pictures show somewhat more sharply defined features than do the model results. These include narrower ridges around expanding holes and smaller satellite droplets than those given by the model. The model uses a number of assumptions that contribute to an overall smoothing effect, including compositional uniformity across the film thickness, a particularly simple law expressing viscosity dependence on composition, an assumed perfectly flat initial layer, and periodic boundary conditions on the computational domain. The small-slope approximation that is inherent in lubrication theory, as used here, is another, relatively minor, source of error.

In addition, the postulated two-term disjoining model used here, must be considered an empiricism, as far as the initial instability is concerned. Once apparent contact lines form, this class of models can incorporate appropriate contact-angle information and permit motion of contact lines for various choices of exponent pairs. This fact was demonstrated by us in a droplet breakup simulation that was accompanied by experimental confirmation (11). There (3, 2) and (4, 3) models were compared with the Lennard–Jones-based (9, 3) exponent pair used by others (13, 14). Each model was shown to provide an adequate fit to the experimental data. For a wetting layer of 50-μm thickness and an assumed perfectly uniform composition, however, no model that is based on molecular interactions can be expected to be the explanation for the initial instability. In the experiment, we believe that it is the finite size of the wax particles, the largest of which may be comparable in size to the coating thickness, that causes the initial nucleation.

It has been established that the principal determinant of the reticulation pattern is the location of the "seed" disturbances. Since the seeds used in the model are taken from the experiment, and the fluid flow and drying model appear to capture the most important aspects of the physics, the simulation gives a good match to the experimental profiles until the coating becomes immobile. This is perhaps remarkable since pattern formation, while surely being a deterministic process, embodies the basic attribute of chaos. That is, as time evolves, strong sensitivity to the details of the initial conditions should make long time prediction increasingly difficult (28, p. 320). Apparently, it is the short duration of the experiment, because of rapid drying, that makes quantitative comparison possible. For longer processes, chaotic behavior is expected to become dominant. Even for such cases, however, we believe that the model has the ability to represent the evolving patterns in the sense that statistical measures of the patterns will be correctly predicted.

Possible extensions and improvements to the model can address other forces that can arise in coating flow, as well as more

complex fluid rheology. In addition to the solutal Marangoni effect that is important for solvent-based coatings, the presence of surface-active material can cause surface tractions that drive flow in the liquid film. Common coating mixtures often are shear thinning. A three-constant generalized-Newtonian flow model can be shown to be consistent with the lubrication approximation. Often substrates to be coated have significant surface features. The present model could also be extended to incorporate nonflat substrates. Each of these extensions has been demonstrated in earlier work on related problems (2, 29–31).

ACKNOWLEDGMENTS

REFERENCES

1. Overdiep, W. S., *Prog. Org. Coatings* **14,** 159–175 (1986).
2. Weidner, D. E., Schwartz, L. W., and Eley, R. R., *J. Colloid Interface Sci.* **179,** 66–75 (1996).
3. Eres, M. H., Weidner, D. E., and Schwartz. L. W., *Langmuir* **15,** 1859–1871 (1999).
4. Kodak Web Site, Glossary of film/video terms, Eastman Kodak Company, 1994–2000, *http://www.kodak.com.*
5. Elbaum, M., and Lipson, S. G., *Phys. Rev. Lett.* **72,** 3562–3565 (1994).
6. Sharma, A., and Reiter, G., *J. Colloid Interface Sci.* **178,** 383–399 (1996).
7. Reiter, G., Sharma, A., Casoli, A., David, M.-O., Khanna, R., and Auroy, P., *Langmuir* **15,** 2551–2558 (1999).
8. Sharma, A., and Khanna, R., *J. Chem. Phys.* **110,** 4929–4936 (1999).
9. Thiele, U., Mertig, M., and Pompe, W., *Phys. Rev. Lett.* **80,** 2869–2872 (1998).
10. Konnur, R., Kargupta, K., and Sharma, A., *Phys. Rev. Lett.* **84,** 931–934 (2000).
11. Schwartz, L. W., and Eley, R. R., *J. Colloid Interface Sci.* **202,** 173–188 (1998).
12. Schwartz, L. W., *Langmuir* **14,** 3440–3453 (1998).
13. Mitlin, V. S., *J. Colloid Interface Sci.* **156,** 491–497 (1993).
14. Khanna, R., and Sharma, A., *J. Colloid Interface Sci.* **195,** 42–50 (1997).
15. Oron, A., and Bankoff, G., *J. Colloid Interface Sci.* **218,** 152–166 (1999).
16. Howison, S. D., Moriarty, J. A., Ockendon, J. R., Terrill, E. L., and Wilson, S. K., *J. Eng. Math.* **32,** 377–394 (1997).
17. Frumkin, A. N., *Zh. Fiz. Khim.* **12,** 337 (1938). [In Russian]
18. Deryaguin, B. V., *Zh. Fiz. Khim.* **14,** 137 (1940). [In Russian]
19. Sharma, A., *Langmuir* **14,** 4915–4928 (1998).
20. Padmakar, A. S., Kargupta, K., Sharma, A., *J. Chem. Phys.* **110,** 1735–1744 (1998).
21. Landau, L. D., and Lifshitz, E. M., *"Fluid Mechanics."* Pergamon, Oxford, 1959.
22. Oron, A., Davis, S. H., and Bankoff, G., *Rev. Modern Phys.* **69,** 931–980 (1997).
23. Peaceman, D. W., and Rachford, H. H., *J. Soc. Ind. Appl. Math.* **3,** 28–41 (1955).
24. Conte, S. D., and Dames, R. T., *J. Assoc. Comput. Machinery* **7,** 264–273 (1960).
25. Yanenko, N. N., *"The Method of Fractional Steps."* Springer-Verlag, Berlin/New York, 1971.
26. Moriarty, J. A., and Schwartz, L. W., *J. Colloid Interface Sci.* **161,** 335–342 (1993).
27. Weidner, D. E., Schwartz, L. W., and Eres, M. H., *J. Colloid Interface Sci.* **187,** 243–258 (1997).
28. Strogatz, S. H., "Nonlinear Dynamics and Chaos," p. 320. Addison–Wesley, Reading, MA, 1994.
29. Schwartz, L. W., Moussalli, P., Campbell, P., and Eley, R. R., *Trans. Inst. Chem. Eng.* **76,** 22–29 (1998).
30. Schwartz, L. W., *in* "Advances in Coating and Drying of Thin Films" (F. Durst and H. Raszillier, Eds.), pp. 105–128. Shaker Verlag, Aachen, 1999.
31. Schwartz, L. W., and Roy, R. V., *J. Colloid Interface Sci.* **218,** 309–323 (1999).